Fluctuation-induced forces between rings threaded around a polymer chain under tension

F. M. Gilles,[1,2,3] R. Llubaroff,[1,4] and C. Pastorino[1,2,*]

[1]*Departamento de Física de la Materia Condensada, CAC-CNEA, Av. Gral. Paz 1499, 1650, Pcia. de Buenos Aires, Argentina*

[2]*CONICET, Godoy Cruz 2290 (C1425FQB), Buenos Aires, Argentina*

[3]*Instituto de Investigaciones Fisicoquímicas Teóricas y Aplicadas (INIFTA), Departamento de Química, Facultad de Ciencias Exactas, Universidad Nacional de La Plata, La Plata 1900, Argentina*

[4]*Facultad Regional Avellaneda, Universidad Tecnológica Nacional (UTN-FRA), Buenos Aires, Argentina*

(Received 18 May 2016; published 14 September 2016)

We characterize the fluctuation properties of a polymer chain under external tension and the fluctuation-induced forces between two ring molecules threaded around the chain. The problem is relevant in the context of fluctuation-induced forces in soft-matter systems, features of liquid interfaces, and to describe the properties of polyrotaxanes and slide-ring materials. We perform molecular-dynamics simulations of the Kremer-Grest bead-spring model for the polymer and a simple ring-molecule model in the canonical ensemble. We study transverse fluctuations of the stretched chain as a function of chain stretching and in the presence of ring-shaped threaded molecules. The fluctuation spectra of the chains are analyzed in equilibrium at constant temperature, and the differences in the presence of two-ring molecules are compared. For the rings located at fixed distances, we find an attractive fluctuation-induced force between the rings, proportional to the temperature and decaying with the ring distance. We characterize this force as a function of ring distance, chain stretching, and ring radius, and we measure the differences between the free chain spectrum and the fluctuations of the chain constrained by the rings. We also compare the dependence and range of the force found in the simulations with theoretical models coming from different fields.

DOI: 10.1103/PhysRevE.94.032503

I. INTRODUCTION

Fluctuation-induced forces have attracted an enormous amount of attention beginning with the renowned Casimir effect, which was discovered in the context of quantum electrodynamics [1]. However, the key elements for the existence of fluctuation-induced forces are present in a broad range of systems. Those elements are a fluctuating medium and an external object, whose presence inhibits or hinders the natural fluctuations of the medium [2]. The first realm of study of fluctuation-induced forces was given by quantum fluctuations of the electromagnetic field with restrictions imposed by perfect parallel conducting plates, as in the seminal work by Casimir [1,3]. However, forces arising from thermal fluctuations of the electromagnetic field have also been predicted and measured experimentally [4]. A variety of physical systems were found to present effective forces of the same origin due to thermal fluctuations of material fields and molecules. For example, colloids located at liquid-liquid interfaces act as physical restrictions of interface fluctuations. Fisher and de Gennes noted that these interactions should appear in a film of a binary liquid mixture close to a wall at the critical point, where the correlation of concentration fluctuations diverges [2,5]. The objects restricting fluctuations are in this case the interface with the wall and the gas-liquid film interface, which are affected by an attractive fluctuation-induced force. This force, known as the critical Casimir effect, was measured recently using colloids and total reflection microscopy [6,7]. Beyond being a fascinating physical effect [8], the fluctuation-induced forces became relevant in practice due to the miniaturization and manipulation of matter at the nanoscale. This ranges from the development of micro- and nanoelectromechanical systems (MEMS) [3] and the behavior of colloids or proteins in interfaces and membranes [2,9–12]. The range of the force is related to the characteristic length of correlation of fluctuations, which becomes comparable with mesoscopic distances between colloids, molecules, or aggregates in many systems. Fluctuation-induced forces have been studied in superfluid films [13,14], liquid crystals, inclusions or proteins in membranes [11,15,16], and colloids confined in liquid interfaces [2,9,10,17,18]. More recently, Casimir-like forces were studied in out-of equilibrium diffusive systems [19] and active matter [20,21].

Within the context of soft matter, we study the fluctuation-induced forces between ring molecules threaded around a polymer chain under tension at thermal equilibrium. The system is interesting from a basic point of view, but it can also be synthesized in the form of supramolecular aggregates, the so-called polyrotaxanes. A polyrotaxane is formed by a varying number of ring molecules, usually cyclodextrin, threaded in a backbone linear polymer chain [22]. The end groups of the polymer are big enough such that the rings cannot get out of the chain, or they are called pseudo-rotaxanes, when the bulkier end beads are not present [22,23]. Novel materials called topological gels have been produced with melts of polyrotaxanes by cross-linking two α-cyclodextrin molecules belonging to different rotaxanes [24]. These eight-shaped links are then movable through the backbone of the polymers, unlike the chemical gels, which have fixed cross-links. Topological gels refer usually to polymer melts in a solvent, but polyrotaxane aggregates with movable cross-links can also be produced with a dry polymeric matrix, thus they are called slide-ring materials [24–26].

In this work, we study the properties of a fluctuating chain under tension with and without threaded rings fixed at given

*pastor@cnea.gov.ar

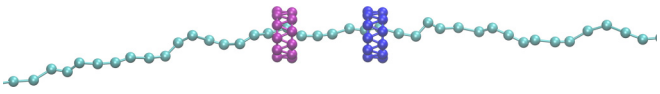

FIG. 1. Snapshot of the system close to the rings, as given by the simulations. The rings are fixed at a distance d. The polymer chain fluctuates at thermal equilibrium in the canonical ensemble. A typical chain has $N = 1024$ beads, and the chain ends are connected through periodic boundary conditions. The links show bond connections for rings and chain given by the FENE model (see Sec. II).

positions, which act as physical constraints of the fluctuation of the chains. The physical system we deal with is shown in Fig. 1, with a typical configuration of the chain-ring system. For the polymer chain without rings, we find a transversal fluctuation spectrum compatible with $\sim 1/q^2$ dependence at high stretchings, and a deviation from it at shorter chain stretchings. We show how this spectrum is modified by the presence of two rings fixed in space, and the appearance of an attractive fluctuation-induced force between the rings. The details of the model and simulation techniques are explained in Sec. II, and we present the results for the fluctuation properties of the chain as a function of chain extensions and temperatures in Sec. III A. We devote Sec. III B to a characterization of the fluctuation-induced forces between the rings as a function of chain extension and temperature. We also compare the dependence of the force with the rings' distance to models of different fields, such as classical electromagnetism and liquid-liquid interfaces. In Sec. IV, we provide a final discussion and conclusions.

II. MODEL AND SIMULATION TECHNIQUES

We use the widely known and studied Kremer-Grest model [27,28] for the polymer chain under tension. The interaction between neighboring beads along the polymer chain is modeled by a finitely extensible nonlinear elastic (FENE) potential:

$$U_{\mathrm{FENE}} = \begin{cases} -\frac{1}{2}kR_0^2 \ln\left[1 - \left(\frac{r_{ij}}{R_0}\right)^2\right] & \text{for} \quad r_{ij} \leqslant R_0, \\ \infty & \text{for} \quad r_{ij} > R_0, \end{cases} \tag{1}$$

where the maximum allowed bond length is $R_0 = 1.5\sigma$, the spring constant is $k = 30\varepsilon/\sigma^2$, and $r_{ij} = |\mathbf{r}_i - \mathbf{r}_j|$ denotes the distance between neighboring monomers. Excluded volume interactions at short distances and van der Waals attractions between beads are described by a truncated and shifted Lennard-Jones (LJ) potential:

$$U(r) = U_{\mathrm{LJ}}(r) - U_{\mathrm{LJ}}(r_{\mathrm{c}}), \tag{2}$$

with

$$U_{\mathrm{LJ}}(r) = 4\varepsilon\left[\left(\frac{\sigma}{r}\right)^{12} - \left(\frac{\sigma}{r}\right)^{6}\right], \tag{3}$$

where the LJ parameters ε and σ define the units of energy and length, respectively. Temperature is given in units of ε/k_B, with k_B being the Boltzmann constant. $U_{\mathrm{LJ}}(r_{\mathrm{c}})$ is the LJ potential evaluated at the cutoff radius. We used standard values for the LJ parameters and mass: $\sigma = 1$, $\varepsilon = 1$, and $m = 1$. The interaction cutoff is located at the minimum of the LJ potential, $r_{\mathrm{c}} = 2^{\frac{1}{6}}\sigma$, which gives effectively a fully repulsive potential and is typical of good solvent conditions when studying polymer melts [29,30]. This model has been applied to a variety of thermodynamic conditions, chain lengths, and physical regimes, such as glasses, melts, dilute solutions, etc. [31–33]. It has also been used for the study of single polymer chains under tension, in a similar physical situation to that studied here, with a focus on dynamical and relaxation properties [34]. The polymer chain was maintained under tension by connecting beads 1 and N through a FENE potential. Periodic boundary conditions were applied by computing the force on each of these beads with the periodic image of the other one. In this way, the length of the chain is set with the box dimension L_x in the $\hat{x}$ direction. In addition, the center of mass of the chain was kept fixed at the center of the MD box.

The ring molecules were generated at fixed positions within the boundaries of the simulation box, and the positions of their beads were not allowed to evolve in time. They were modeled by groups of 11 beads, arranged in two parallel circles. This number was chosen because we found it to be the minimal number of beads at which the rings did not unthread from the chain for different chain stretchings and temperatures. We chose the beads of the rings to be the same size as the beads of the chain for simplicity. We do not attempt to develop a detailed model of an annular molecule. The ring molecules are meant to provide a consistent physical constraint for the transverse fluctuations of the polymer chain. Beads in the rings are connected by springs (see Fig. 1) with the same FENE interactions that we used for the connectivity of the chains. In the model of the ring molecules, it was necessary to use two interlocked groups of beads, because setting only one is prone to unthreading from the chain at high stretchings or temperatures (see Fig. 1). The excluded volume of beads was also described by a LJ potential, also with a cutoff of $r_{\mathrm{c}} = 2^{\frac{1}{6}}\sigma$, which keeps only the repulsive part of the LJ potential. The interaction of the rings with the chain is therefore purely repulsive, as is the interaction among beads of the rings. This rules out any direct attractive interaction between rings, which is important to isolate the effective interaction arising from the Casimir-like forces.

We used a Langevin thermostat to study the system at constant temperature. Dissipative and stochastic forces are added to the conservative forces that are already present in the standard molecular-dynamics equations of motions. The dissipative force on particle i is given by $\mathbf{F}_i^{\mathrm{D}} = -\gamma\mathbf{v}_i$, where γ is the friction coefficient and $\mathbf{v}_i$ is the particle velocity. The random force, $\mathbf{F}_i^{\mathrm{R}}$, has zero mean value, and its variance satisfies [35,36]

$$\left\langle F_{i\mu}^{\mathrm{R}}(t) F_{j\nu}^{\mathrm{R}}(t')\right\rangle = 2\gamma T k_B \delta_{ij}\delta_{\mu\nu}\delta(t - t'), \tag{4}$$

where the indices i and j label particles, μ and ν are Cartesian components, and T is the temperature at which the system is simulated.

After a thermalization stage of 1×10^6 MD steps with a time step of $dt = 1\times10^{-5}\tau$, typical simulations were performed with trajectories of 1×10^7 MD steps each, with a time step of $dt = 2\times10^{-3}\tau$. The time unit in LJ parameters is $\tau = \sigma(m/\varepsilon)^{1/2}$. We took averages of physical quantities each

1000 time steps. The friction constant was set to $\gamma = 0.5\varepsilon\tau/\sigma^2$ for all the simulations except for the initial thermalization stage, in which the friction constant was set to $\gamma = 50.0\varepsilon\tau/\sigma^2$. The typical chain was composed of $N = 1024$ beads, but we also studied shorter and longer chains when needed. These cases will be mentioned explicitly in the text. This choice allowed us to study ring distances in the range 3–60σ in order to obtain fluctuation-induced force values with a high enough signal-to-noise ratio.

III. RESULTS

A. Properties of the polymer chain under tension

We analyze first the structural and fluctuation properties of the chain under extensional force, without rings. We worked with simulations at constant length, giving rise to a mean constant stretching force. Figure 2 shows typical configurations of the chains for different extensions. The chain length is given in units of the maximum extension of the FENE model chain, $L_{\max} = 1.5N\sigma$. For the smaller extensions, the chain starts to show a blob formation. There are local regions of beads arranged in configurations not very different from that of isolated chains (Fig. 2, $L^* = 0.4$). For larger extensions, the chain is very stretched, with little freedom for transverse relative displacement among consecutive beads (Fig. 2, $L^* = 0.70$). In this regime, the internal energy of the chain is very high, and it is dominant compared to configurational entropy.

This behavior can be quantified with the mean bond length in units of the maximum allowed bond length for the FENE model ($R_{\max} = 1.5\sigma$). This is shown in Fig. 3 as a function of chain stretching, for different temperatures. For stretchings in the range $L^* < 0.65$, the mean bond is marginally dependent

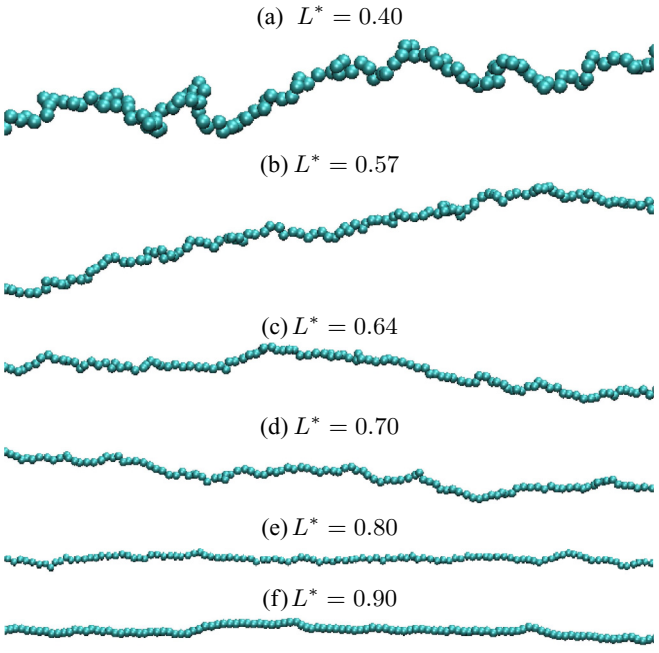

FIG. 2. Snapshots of a fragment of the polymer chain at different extensions and temperature $T = 33.6\varepsilon/k_B$. L^* accounts for the length as a fraction of the maximum possible chain extension in the FENE model, $L_{\max} = 1.5\sigma N$.

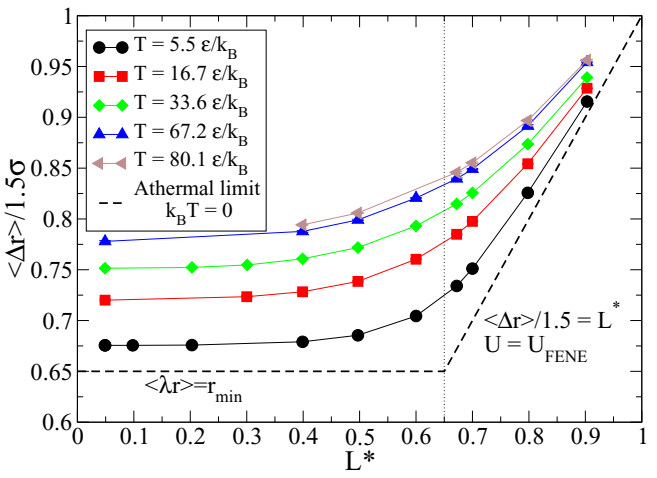

FIG. 3. Mean bond length as a function of chain stretching for different temperatures in units of maximum FENE length. The dashed line represents bead distance in the limit of $k_BT = 0$ and no excitations in the chain (athermal limit). The vertical dotted line indicates the extension at which the bond length increases its rate of change with chain stretching.

on chain length, and it increases toward the limit $L* \simeq 0.65$. In this regime, the blobs are dominant and the bond length values are dominated by the thermal energy of the beads and the excluded volume, which is given by the Lennard-Jones potential. In the case $L^* \gtrsim 0.65$, the bonds increase more pronouncedly with chain stretching. In this limit, each bond is permanently stretched with respect to the equilibrium bond length, and the excluded volume is not important for the mean bond. For very high L^*, the bonds converge to the maximum value for all the temperatures. The case $T = 0$ (athermal) is shown for comparison with a dashed line. This is the limiting case, in which there is only potential energy in the chain. This is in agreement with the behavior of the thermal case, indicating also the two distinctive behaviors. The value $r_{\min} \sim 0.65$ corresponds to a bond distance $d = 0.975\sigma$, where the Lennard-Jones and bond forces are equal. Figure 4 shows the bond distance as a function of temperature for different chain extensions. The mean bond is more dependent on temperature at shorter chain extensions and lower temperatures. The FENE contribution of the bond energy is, of course, nonlinear, and therefore the temperature has a progressively minor effect with increasing temperatures.

We also calculate the spectra of transverse fluctuations of the chain (i.e., those perpendicular to the stretching direction $\hat{x}$) to characterize the collective vibrations in the limit of high stretching. We point out that even the lowest stretching case ($L^* = 0.20$) is still very high as compared with a free polymer chain. We define a discrete function $h(x_i) = h_{\text{bin}}(x_i) - h_0$, which accounts for the transverse fluctuations. h_{bin} is obtained by dividing the space along the chain in bins of width $\Delta x = 2\sigma$ and then computing the mean position of the beads that belong to each bin. This binning procedure was used because for short chain lengths the beads are grouped in blobs, and taking their positions directly would give a multivalued function at some x points. This type of discretization is usual in an analysis of interface fluctuations [30,38]. h_0 is the horizontal along the

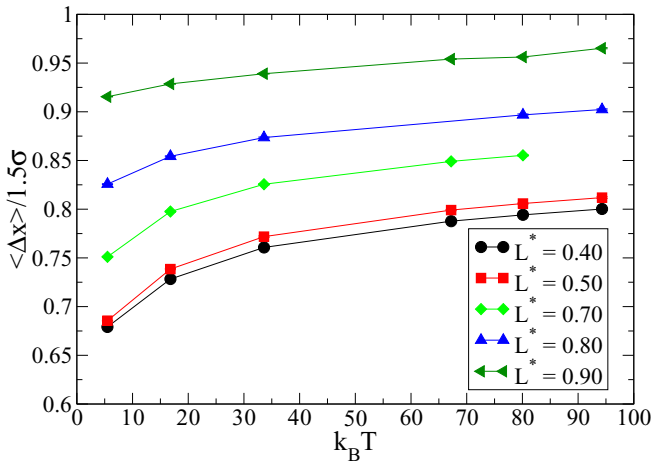

FIG. 4. Mean distance among beads as a function of temperature for different chain extensions. A saturation at higher temperatures is observed in accordance with the fast increase of FENE bond energy.

x direction, in which would lie the stretched chain at zero kinetic energy. For each time step, the Fourier amplitudes are calculated and averaged over the chain configurations obtained in the simulations. The fluctuation spectra, given by the square amplitude of the Fourier modes, are shown in Fig. 5 for some selected chain lengths. The inset shows the power spectra in logarithmic scale. The overall magnitude of fluctuations is, as expected, reduced with chain stretching. The wave amplitudes also decrease with q number or, equivalently, increase with wavelength λ.

In the limit of very high stretching, the harmonic approximation should hold due to the small-amplitude oscillations of the beads, which are effectively trapped in very stiff potential wells. This can be thought of as an effective Hamiltonian with quadratic degrees of freedom in coordinates and momenta. The chain is in a heat bath at constant temperature, and therefore the equipartition theorem holds, giving a contribution of $\frac{1}{2}k_BT$ for each degree of freedom to the potential and kinetic energies. Each normal mode of the chain has the same mean

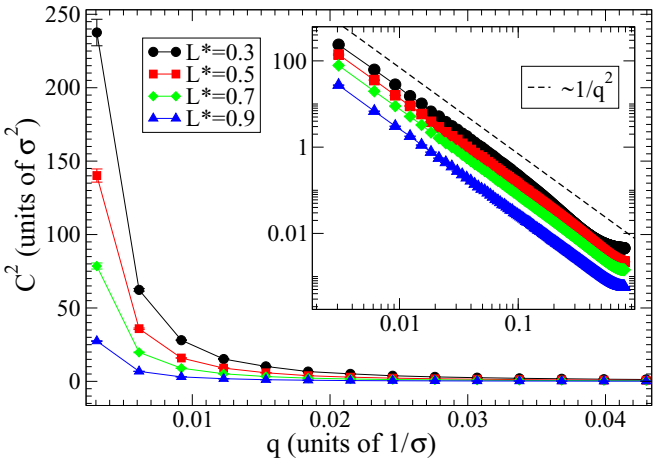

FIG. 5. Fourier spectrum of the polymer chain at different lengths for $T = 33.6\varepsilon/k_B$. The inset shows the same data in log-log plot.

potential energy of $\frac{1}{2}k_BT$, and, by using the relation between the potential energy of a mode and the amplitude [37], the harmonic model gives rise to a dependence of the squared mode amplitude $C^2 \sim 1/q^2$. The same conclusion can be reached in the realm of soft matter and interfaces for a capillary wave Hamiltonian. The fluctuating stretched chain projected in a plane can be thought of as a unidimensional interface between two immiscible liquids or a liquid-gas interface, and the modes of the chain can be thought of as the capillary waves of the interface. The energy cost of a nonflat surface in comparison to the flat case (of minimum area) can be written as an effective Hamiltonian of surface fluctuations. This so-called capillary wave Hamiltonian describes the energy cost of surface undulations of thermal origin in terms of a function $h(x,y)$, which accounts for the local position of the interface. Expressing this Hamiltonian in Fourier space leads to a quadratic form in the wave vectors q of independent harmonic oscillators. The application of the equipartition theorem leads to the dependence $C(q) \sim k_BT/q^2$ for the Fourier amplitudes of the Fourier modes of the surface [38,39]. This analogy is very interesting because simulations can test which range of chain extensions is valid, and it enables the study of interface fluctuations by carefully simulating a stretched chain. The chain is, of course, much less demanding of computing power. The dashed line in the inset of Fig. 5 shows a curve $\sim 1/q^2$ for reference. For the higher extensions ($L^* = 0.90$ and 0.70), the chain fluctuations are very close to the harmonic model. The curves are parallel to $1/q^2$ for the whole range of q. Some differences show up for the smaller extension, $L^* = 0.40$, which increase appreciably for the lowest stretching, $L^* = 0.20$. This is especially true for the high-q part of the spectra, i.e., for the shorter-wavelength modes. Interestingly, this is in line with the idea of the capillary wave Hamiltonian (also the Helfrich Hamiltonian, for membrane bilayers). These models are suitable for long-wavelength fluctuations [38,39]. We recall that for the shorter chain lengths, the Lennard-Jones interaction, i.e., the excluded volume, has a role in the local dynamics of the beads.

Figure 6 show the decaying exponent of the spectra for different chain stretchings and temperatures. We fitted the function $f(q) = A_0/q^\alpha$ in the log-form, where A_0 and α are the fitting parameters. A convergence toward $\alpha = 2$ is observed upon an increase of chain stretching. For the range of shorter chain stretchings ($L^* < 0.5$), the exponent increases. This means a deeper decay of fluctuations for smaller wavelengths. For these lower stretchings the polymer chains are more intertwined, and the vibrational behavior comes more from groups of beads than from independent beads themselves. This could be thought of as an effectively shorter chain (with fewer degrees of freedom, and therefore modes), and for the same q range of the complete chain it will have a faster decay.

B. Effect of the rings on the chain and fluctuation-induced forces

We analyze here the effect of the fixed rings in the natural fluctuations of the chain, after which we will proceed to the fluctuation-induced or Casimir-like forces between rings. Figure 7 shows the fluctuation spectra of the chain with

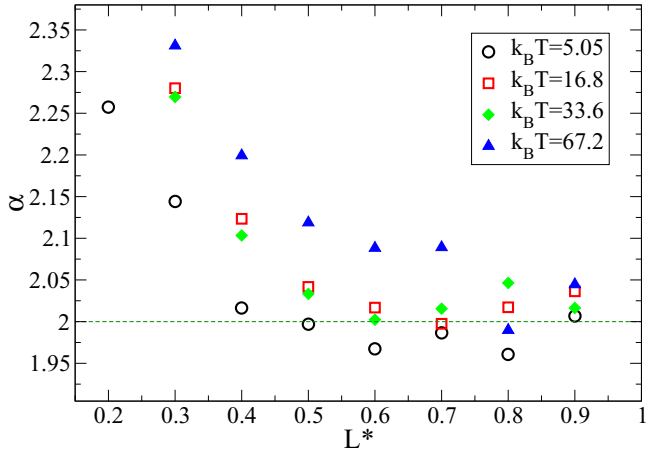

FIG. 6. Exponent of the fitted decay of the fluctuation spectrum as a function of chain length for different temperatures. From the capillary-wave Hamiltonian, a coefficient $\alpha = 2$ is expected (indicated with a dashed line). The exponent gets closer to $\alpha = 2$ from $L^* = 0.5$ toward higher stretching values.

the rings fixed at different distances. The decay range is similar for the chain with and without rings, but the modes whose wavelengths are higher than the distance between rings ($\lambda_{\text{mode}} > d$) are significantly reduced. The power spectrum of the chain without rings is shown also for comparison.

Figure 8 shows the difference in the power spectrum with and without rings for different ring distances. The effect of the rings is clearly observed for the modes that are expected to be heavily hindered by the rings. The higher effect is observed for smaller distances in which modes of lower wavelengths are reduced, starting at $\lambda_{\text{min}} = d$. It is also observed that increasing the ring distance changes the cutoff wave number from which the spectrum is significantly reduced, as compared to the stretched chain without rings.

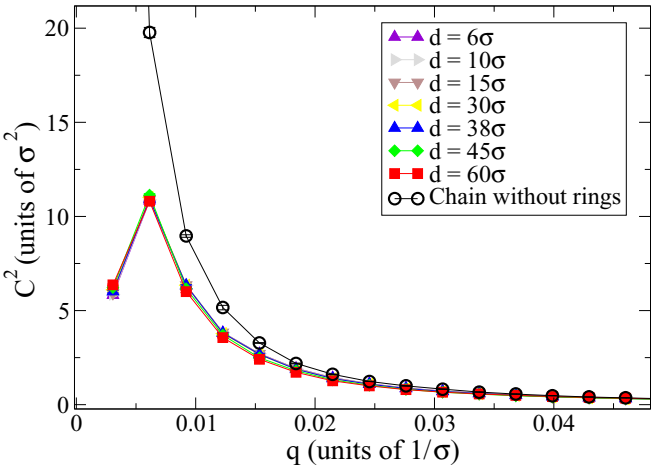

FIG. 7. Fourier spectrum for the chain without rings (open circles) and with the rings located at different distances (filled symbols). All the cases correspond to $T = 33.6\varepsilon/k_B$ and $L^* = 0.70$. The effect of the rings is only noticeable at small q (long wavelengths) and it becomes unnoticeable at high q values.

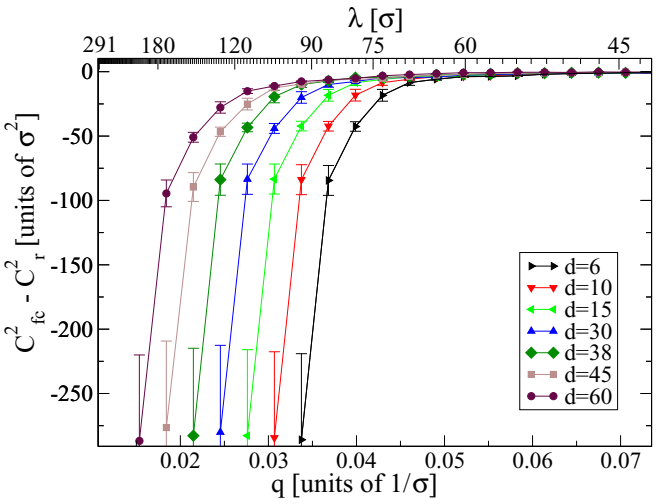

FIG. 8. Difference of Fourier coefficient normalized sum for the case of the chain with rings (C_r^2) and the chains without rings (C_{fc}^2). The legends show the distance between rings at which the spectra were calculated. The vertical line indicates the q value ($\lambda \sim 67\sigma$) below which the presence of rings begins to influence the amplitude of the chain modes. The cutoff of modes at $q \lesssim 2\pi/d$ produced by the presence of the rings is clearly appreciated.

In Fig. 9, the mean number density of the chain is presented. Panel (a) shows the chain without rings, while panels (b) and (c) present the changes for rings located at distances 30σ and 6σ, respectively. We obtained the histograms from a square binning in two dimensions with a bin lateral size of $\Delta r = 0.25\sigma$, and a Bessel smoothing function was used for the color plots. The spatial zone at which the beads have access

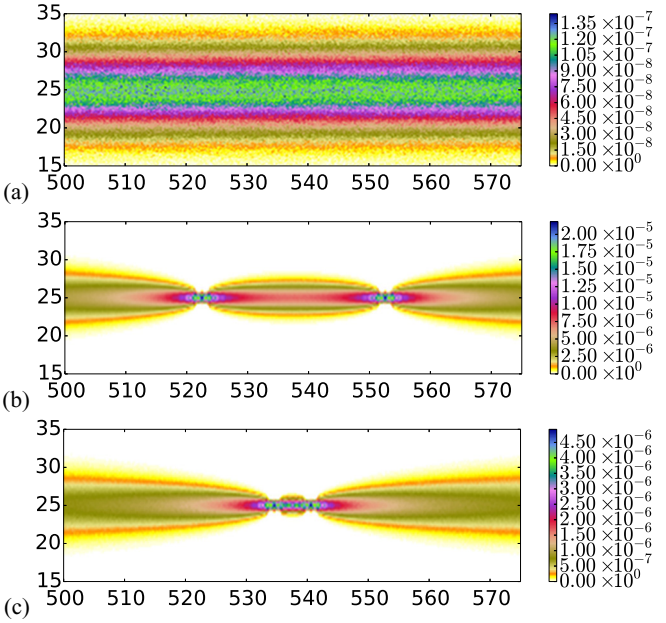

FIG. 9. Color plot of the number density for the central zone of the chain. Panel (a) presents the chain without rings. The density with rings at distance $d = 30\sigma$ is presented in panel (b), and the density with rings at $d = 6\sigma$ is presented in panel (c).

is significantly reduced by the presence of the rings. This is in line with the suppression of modes of higher amplitude in the presence of rings. For the zone between rings, the bead distribution is similar to the outer zone for high ring distances [panel (b), $d = 30\sigma$], but with reduced amplitudes. For rings very close [panel (c), $d = 6\sigma$], the inner zone presents beads only very close to the rings. The outer zone, however, presents monomers in a slightly wider zone as compared to the case of rings located at higher distances [see panel (b) in Fig. 9], compatible with the fact that the outer zone of the chain can have modes of very high wavelength and amplitude (see Sec. III A) when the rings are very close to each other.

In addition to the fluctuation properties of the chain, we found another interesting aspect that changes in the presence of fixed ring molecules. We studied the mean bond length for all the chain bonds, considering separately the bonds lying between the rings and those in the outer region. Figure 10 depicts the mean bond lengths obtained from the mean bond value over neighboring beads in the chain. The pair number is defined such that pair number i indicates the bond between beads $i + 1$ and i. Figure 10 provides an example of what we have observed for all the cases. First, there is a significant stretching of the bonds that are directly exposed to the fixed rings. This can be expected: as the chain fluctuates, the bonds will scatter against the beads of the rings, producing a high stretching of these bonds. There is also a much more subtle and interesting effect, which we noticed for different stretchings and temperatures. Namely, the bonds between rings are slightly stretched on average. This can be observed in the center points of Fig. 10, which are systematically above the dashed line. This indicates the mean bond value for the bonds in the outer region of the chains (those in the regions of bond numbers 1–503 and 522–1023). The chain is more stretched between rings. From a mechanical viewpoint, we attribute this to the action-reaction principle. As will be shown next, the chain is effectively producing a mean force between rings, and there should be a force equal in magnitude that the rings exert on the chain, giving rise to this slight increase of the bond length in the zone between rings. This interesting characteristic could be explored further, but this is beyond the scope of the present work.

The nature and characteristics of the effective forces between rings are one of the main results and motivations of our study. We compute the mean force on each bead of the rings, averaged over each MD step. This quantity is the mean force on the ring due to the interaction with the chain. We recall that ring-ring interaction is neglected because we used a cutoff for the ring-ring interaction of $R_c = 1.12\sigma$ among beads of the same and different rings. We kept only the repulsive part of the Lennard-Jones potential, which means that only the excluded volume is considered. As rings were fixed at distances $d \geqslant 3\sigma$, direct interactions between rings are disregarded by design. We show in Fig. 11 one of the main results of this work, namely the existence of an effective force between rings that can only arise through interactions mediated by the chain. Furthermore, the rings are able to hinder transverse fluctuations of the chains, but not longitudinal waves, since the effective ring diameter is bigger than the bead diameter of the chain (1σ). We conclude that this effective interaction is the expected fluctuation-induced force due to the disturbance of the natural fluctuations of the stretched unconstrained chain by the presence of the rings. They have a range clearly larger than the ring size ($\sim 6\sigma$). Another qualitatively important aspect is that the interaction is attractive for all the studied cases. We point out also that the nature of the system disregards other types of effective interactions, such as, for example, depletion interactions, which are usually present together with fluctuation-induced forces in many systems [40]. From a thermodynamic viewpoint, the system minimizes free

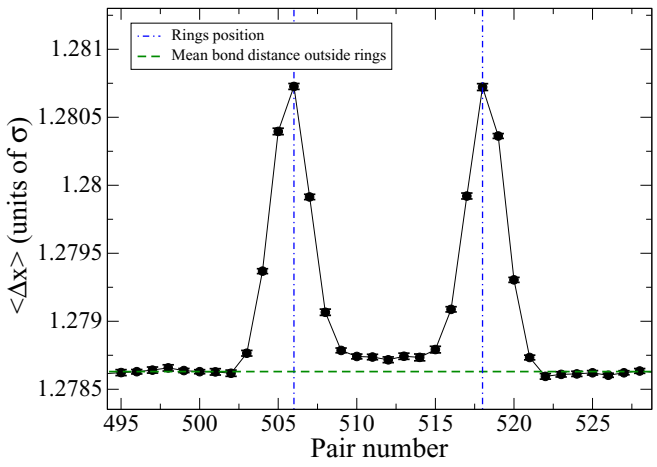

FIG. 10. Mean bond lengths $\langle \Delta x \rangle$ as a function of bond number for different polymer lengths. The rings are located at $d = 15\sigma$ with a chain stretching of $L^* = 0.8$ and temperature $T = 15\varepsilon/k_B$. The bond number is labeled such that the bond number b_i is the bond distance between beads $i + 1$ and i. Vertical dot-dashed lines indicate the approximate position of the rings. The error bars are almost the same size as the symbols.

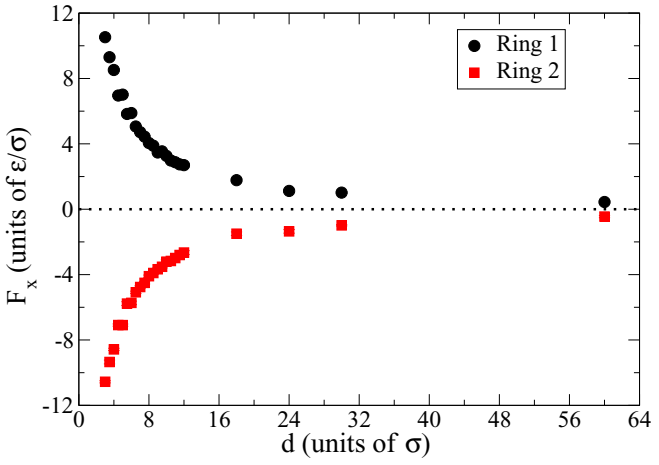

FIG. 11. Total mean force on rings $\langle f_{\text{ring}}^{(x)} \rangle$ in the chain direction as a function of ring distance. Each annular molecule is composed of two rings formed by 11 LJ particles located on a circle of radius 1.5σ. The sample was set at $T = 33.6\varepsilon/k_B$ and $L^* = 0.70$. These are the fluctuation-induced or Casimir-like forces from the chain on the annular molecules, due to the restrictions that they impose in the natural fluctuations of the chain. For a given distance, the rings hinder the fluctuations of the chain with modes of wavelength $\lambda > d$.

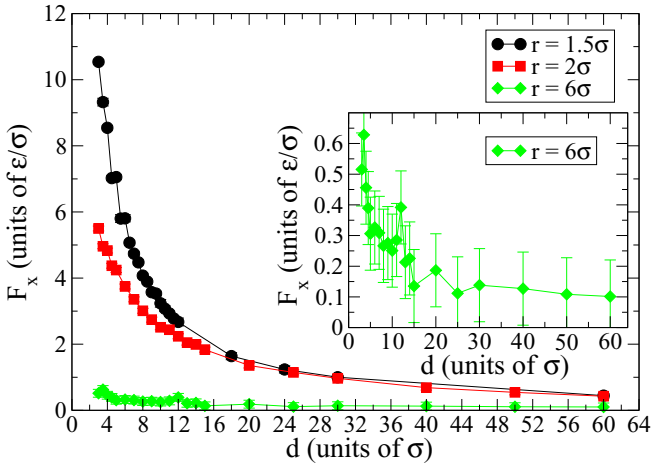

FIG. 12. Mean force between rings vs distance for different ring radius r. The parameters were set as $L^* = 0.70$ and $T = 33.6\varepsilon/k_B$. The inset shows a magnification of the case $r = 6\sigma$, for which the minimal restrictions imposed by this big ring radius reduce significantly the fluctuation-induced force.

energy with the rings as close as possible to each other. This allows for modes with longer λ in the outer region. However, as we have the chain in a thermal bath (a canonical ensemble), the mean internal energy of the chain is the same for all the cases. Therefore, the Casimir-like force arises in particular from the maximization of entropy, which is obtained when the rings are together. Entropy is maximized when the maximum possible number of modes are active, particularly those of higher amplitude (high λ; see Sec. III A). As we showed earlier, these modes are hindered when the rings are placed at higher distances.

The ring molecules are of course physical constraints and not mathematical nodes imposed on the chain. It is helpful to analyze the fluctuation-induced force as a function of ring radius. This is done in Fig. 12, where we plot force versus ring distance for different ring radii. The force is present in all cases, but it is greatly reduced for larger ring radii. The inset shows a zoom of the larger radius ($r_{\text{ring}} = 6\sigma$), which is barely noticeable in the scale of the main graph. As the ring radius increases, the rings are unable to hinder the fluctuations of middle to small wavelength, which are progressively of smaller amplitude as λ decreases. The ring radius modifies significantly the strength of the fluctuation-induced force.

We present in Fig. 13 the force strength between rings for different chain stretchings and temperatures as a function of distance. Panel (a) presents the force intensity versus distance. The force is long range as compared to bead size. We resolve nonzero force values up to $d \simeq 48\sigma$ for a chain length of $L = 1076\sigma$ and 1024 beads. The force is non-negligible approximately for distances in a range of 5% of the chain length. For short ring distances, Fig. 13 shows that the strength of the force is highly influenced by the amplitude of the chain modes of higher wavelength. As was shown for the fluctuations of the chain without rings (see Fig. 5), less stretching increases considerably the amplitude of the modes in the small q range (longer wavelengths). With higher chain stretchings, for instance $L^* = 0.8$ in Fig. 13(a), an oscillation of the force

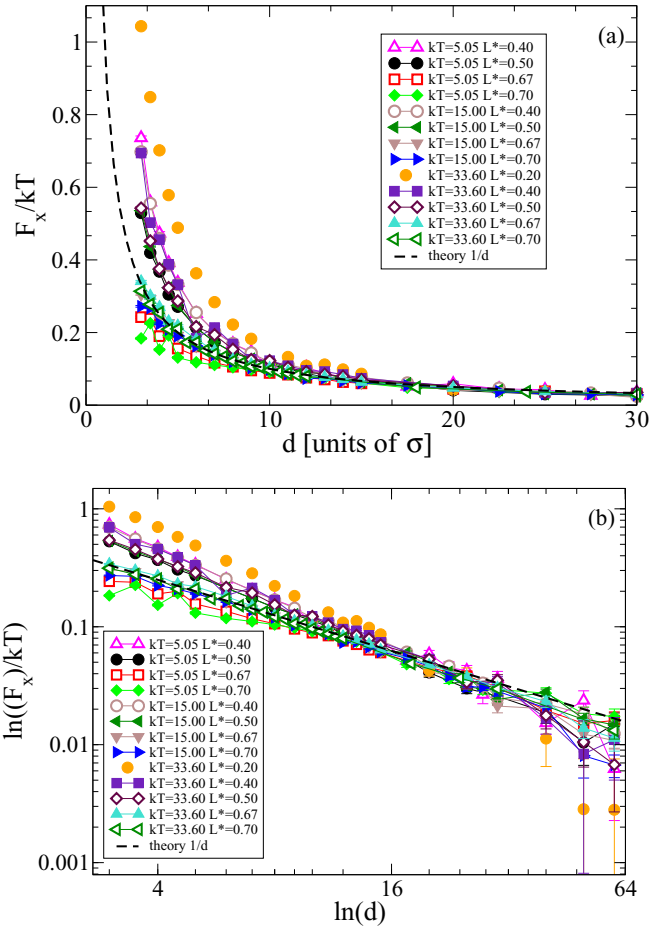

FIG. 13. Upper panel: mean force vs ring distance for different chain stretchings and temperatures. The dashed line represents the harmonic model for the force $f \sim 1/d$. It indicates only the power-law decay. Lower panel: log-log plot for the same cases. The dashed line shows an idealized theoretical model that is consistent for medium to high stretching (see the text).

occurs, which is noticeable at shorter ring distances. We will analyze this further in the next paragraphs.

Comparison with theoretical models

To compare the force with analytical models, we provide a log-log plot of the force scaled with the temperature in Fig. 13(b). First, we fitted the force between rings as a function of distance as a power law of the form $F(d) = A(T)/d^{\alpha}$. A log-log plot should present a linear dependence, which is approximately the case in Fig. 13(b). The exponent α changes with chain stretching, growing for smaller L^*. The dashed line represents the case $\alpha = 1$, which can be obtained analytically with a harmonic approximation of independent normal modes [41,42]. Boyer discusses the standard Casimir effect from zero-point energy fluctuations of the electromagnetic field and thermal fluctuations of the classical electromagnetic field in a unified way [41,42]. The latter case is equivalent to the chain in a thermal bath. The system is described as a one-dimensional cavity at a given temperature, with a partition inside the cavity at position x. He calculates the total force on the partition due to the restriction of modes in the cavity.

Considering harmonic modes, the equipartition limit gives rise to a contribution to the force of each normal mode of $f_{\text{mode}}(\omega, L, T) = \frac{k_B T}{L}$, where L is the length of the cavity. Adding up over all the modes, the total force on the partition at position x is

$$f(x, L, T) = -\frac{k_B T}{2}\left(\frac{1}{x} - \frac{1}{L - x}\right),$$

where the two terms indicate attractions to each one of the wall cavities [42]. In our case, the boundary condition is periodic and the force between rings is mapped to the force between the partition and one of the walls. If the partition is close to one of the walls, the interaction with the other one is negligible. This would be the limit of two rings at short distance in comparison with chain length ($d \ll L$), which we use in the simulations. The ring distance varies in a range 2-60σ in a chain of typical length $L = 1076\sigma$. We also add a factor 2 due to two independent fluctuation directions for the chain ($\hat{y}$ and $\hat{z}$), which are locally constrained by the presence of the rings. We end up, therefore, with a force dependence given by

$$F_x(d) \equiv f_{\text{ring}}(d) = \frac{k_B T}{d},$$

which is plotted in Fig. 13 by a dashed line.

Interestingly, the theory agrees fairly well with our results for relatively high chain stretchings ($L^* \gtrsim 0.67$) and for all the studied temperatures. At very high chain stretching, $L^* > 0.7$, there are force oscillations at short ring distances (considered later on), but we have again good agreement with the theoretical model at longer ring distances. It should be noted that the interactions of individual bonds are nonharmonic elastic terms, given by the FENE potential [see Eq. (1)]. However, in the limit of high stretching, we consider that the harmonic approximation is reasonable. We think that this is because each bead of the chain is trapped in a very stiff potential well, which for moderate temperatures could be well approximated by a Taylor expansion of second order. This is in the same spirit of the small-amplitude harmonic approximation of vibrational modes in a solid at relatively low temperature [43].

In the lower range of chain stretchings ($L^* < 0.65$), we do not observe a dependence $\sim 1/d$. We note that in this regime, not all the degrees of freedom of the chain are taking part of the vibrations. The low stretching produces local clusters of beads, closer to equilibrium than to bond stretched states [see Fig. 2(a)]. We attribute to this effective reduction of vibrational modes a steeper decay of the interaction, as compared to the cases of higher stretchings, where the harmonic approximation holds. It is also interesting to note that in this region, the range of the fluctuation-induced force is reduced, but its absolute value at short ring distance increases. We assume that this happens because the amplitude of long-wavelength modes increases significantly for shorter chain stretchings (see Fig. 5). It is worth noticing that the fluctuations of the chain without rings are still closer to $\sim 1/q^2$, characteristic of the capillary wave Hamiltonian. Lehle *et al.* [9] obtained analytical results for the dependence of effective forces in interfaces, induced by capillary wavelike fluctuations. They analyzed colloids trapped in a liquid-liquid interface with different boundary conditions of the colloid-interface and different degrees of freedom of the colloids. They also treated different shapes as spherical, janus colloids, or disks. The different cases included totally fixed colloids pinned in the interface, colloids allowed to move vertically, and colloids allowed to move vertically and also to tilt. The case closer to the system considered here is the fluctuation-induced force between disk colloids of radius r_0, pinned in the interface at distance d. For the limiting case $d \gg r_0$, they find the following expression for the fluctuation induced force [see Eq. (7) in Ref. [9]]:

$$F_x(d) = -\frac{k_B T}{2}\frac{1}{d \ln(d/r_0)} + O(d^{-3}). \tag{5}$$

We fitted Eq. (5) with a multiplicative constant A and $c_1 \equiv 1/r_0$ as fitting parameters, and we found very good agreement for the smaller chain stretchings ($L^* < 0.65$) at different temperatures. Two examples are provided in Fig. 14 for chain lengths of $L^* = 0.4$ [panel (a)] and $L^* = 0.5$ [panel (b)]. The lateral extension of the rings, which can be regarded as the colloid radius r_0, is small compared to the typical ring distance in the simulations, fulfilling the conditions for this limiting case. The fitting parameters are around $A_0 \simeq 4$ for the multiplicative constant of the force and $r_0 \simeq 0.36$ (with

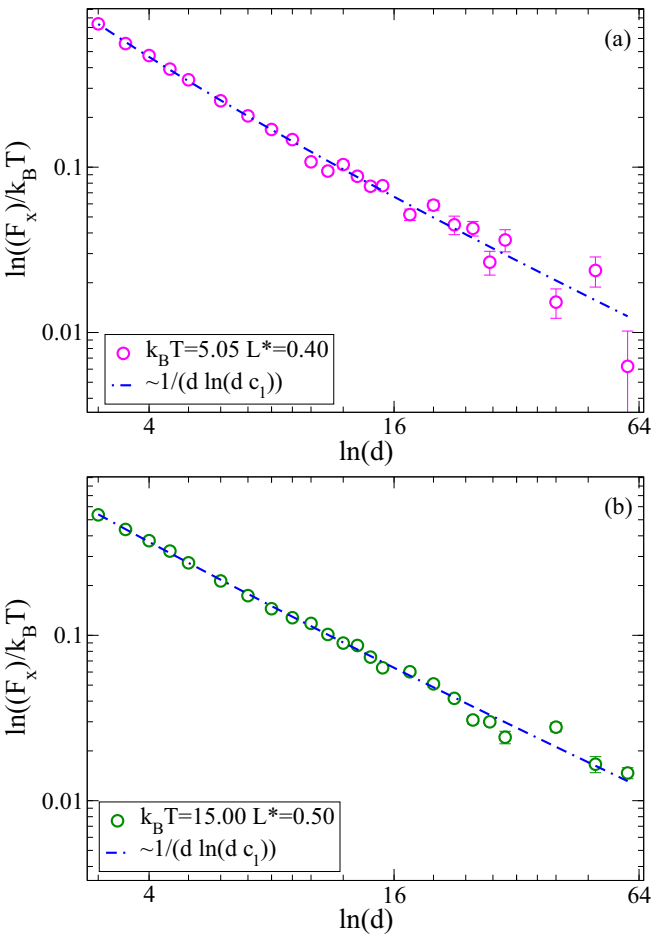

FIG. 14. Fit of the fluctuation-induced forces vs distance for low stretching. They were adjusted with the model of Eq. (5) by Lehle *et al.* [9]. Panel (a) corresponds to the case $L^* = 0.4$ and $T = 5.05\varepsilon/k_B$, while panel (b) corresponds to $L^* = 0.5$ and $T = 15.0\varepsilon/k_B$.

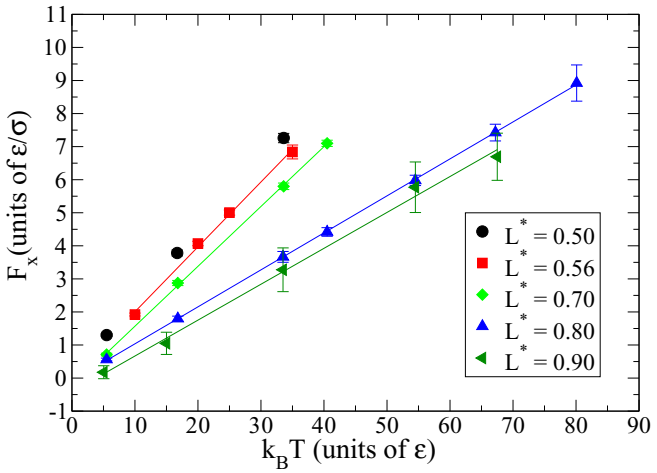

FIG. 15. Force between rings F_x as a function of temperature for different chain lengths L^*. In all the cases, the rings were fixed at a distance $d = 6\sigma$. The lines come from a linear fit of the data point.

$r_0 = 0.14$ and 0.55 as the minimum and maximum values for all the fits). This mean value seems a bit smaller than the effective ring width (in its part exposed to the chain), but it is indeed in the order of magnitude of the effective ring width.

We also studied the dependence of the fluctuation-induced force with the temperature. Figure 15 shows the fluctuation-induced force between rings located at a distance of $d = 6\sigma$ for different chain lengths. The curves present a linear behavior. This is expected, because the fluctuation-induced interactions are proportional to the driving energy of fluctuations, $k_B T$ in our case [44]. We observe also a smaller slope of the curves for higher chain stretching. This fact can be rationalized by considering two facts. On the one hand, the nonlinearity of the bond potential make the bonds effectively stiffer for higher stretching. The rate of increase of mode amplitudes upon an increase in temperature is therefore lower for more stretched chains. On the other hand, the hindering of modes of higher amplitude (low q) seems to be the most important

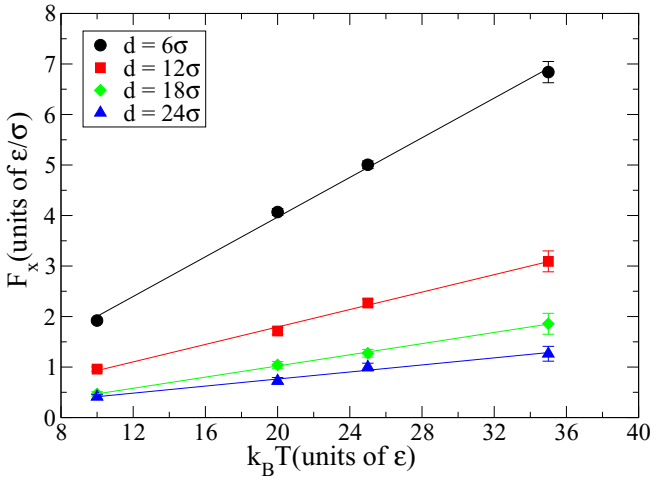

FIG. 16. F_x vs temperature for different ring distances. All the cases correspond to $L^* = 0.56$, and the number of beads in the chain is $N = 1024$. The lines are linear fits of the data for each case.

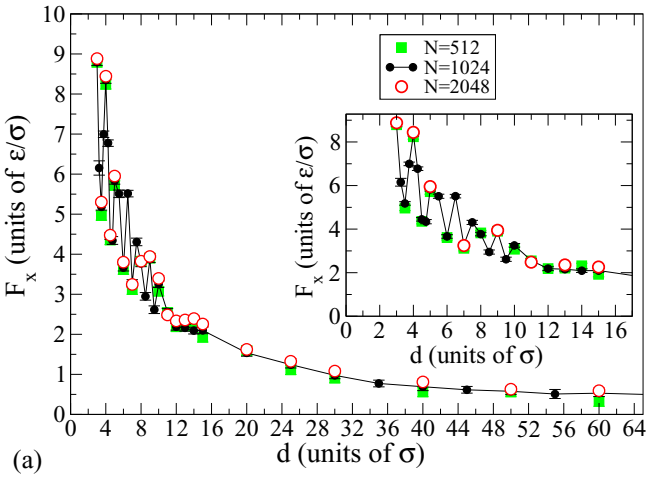

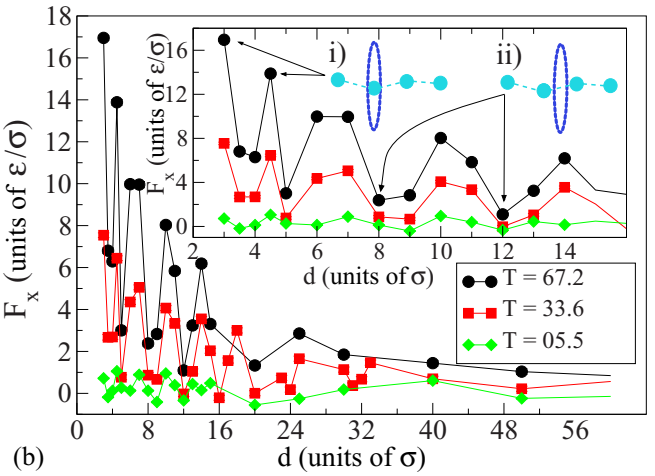

FIG. 17. (a) Force vs distance for different numbers of beads in the chain at the same chain stretching $L^* = 0.80$. (b) F_x as a function of distance for $L^* = 0.8$ at different temperatures. The insets in both panels show a detailed view of F_x for short distances.

contribution to the fluctuation-induced force. This can be observed in Fig. 13 ($d \gtrsim 6\sigma$), where at equal temperature, the force is higher for shorter chains, i.e., for chains of higher low-amplitude modes (see also Fig. 5). These two facts may give rise to the smaller dependence with temperature of more stretched chains observed in Fig. 15.

Figure 16 shows the force at different ring distances as a function of temperature for a fixed chain stretching of $L^* = 0.56$. A linear dependence is also observed in this rather narrow temperature interval. This indicates that the change of the force is dominated by the number of modes, which is the same at larger temperatures, increasing the modes' amplitudes. In a thermodynamic framework, the term $T\Delta S$ of the free energy depends on temperature basically only through the explicit T dependence, and not in ΔS.

Finally, we discuss in more detail the oscillations of the fluctuation-induced force versus distance at very high stretching observed in Fig. 13. In Fig. 17, we show the force versus ring distance for $L^* = 0.8$ for different chain lengths [panel (a)] and different temperatures [panel (b)]. A clear modulation of the force shows up for short distances up to $d \simeq 16\sigma$. This was observed in the high stretching

limit $L^* \gtrsim 0.8$ for all the studied cases. We recall that the maximum physical length that the FENE chain can have is $L^* = 1$, which is quite close to these cases. The beads are rather separated, and the centers of the bonds have a clearly reduced excluded volume compared to positions closer to the center of the beads. In these conditions, for a given ring distance, it makes a significative difference if the rings are located very close to a bead [see inset (i) in Fig. 17] or in the central region of the bond [see inset (ii) in Fig. 17]. In the second case, the chain can have fluctuations of higher amplitude inside the ring, giving rise to a lower fluctuation-induced force. This is also facilitated by the fact that the bond-length lateral fluctuation is rather low due to the high stretching of the polymer and the high internal energy of the bond. We confirmed this by scaling the ring distance with the mean bond distance $\langle l_{\text{bond}} \rangle$ for each case. Plotting F_x versus $d/\langle l_{\text{bond}} \rangle$, we observe a period for the modulation of one bond length (not shown). The modulation smudges at longer ring distances, where lateral displacements of the beads close to the rings are much larger.

While these stretching values are rather extreme and might not be feasible experimentally, they draw attention to the fact that the structure of the bond, and the details of the polymer structure at the chemical level, could have a role in the modulation of fluctuation-induced forces in experiments.

IV. DISCUSSION AND CONCLUSIONS

In this work, we studied the fluctuation properties of a polymer chain under tension and the characteristics of the fluctuation-induced forces between two ring molecules threaded around the polymer and fixed in the space. In this way, the rings alter the natural fluctuations of a stretched chain giving rise to the observed Casimir-like forces. The system could be considered as a model of a pseudo-rotaxane under tension, which could be studied experimentally as an isolated entity, or as a component of a slide-ring material under tension.

The unconstrained chain under tension presents a fluctuation spectrum compatible with a $\sim 1/q^2$ law for a wide range of studied chain stretchings, which deviates from the behavior for lower chain lengths. Interestingly, the behavior at high stretching is similar to a capillary wave spectrum of a liquid-vapor interface or that of two immiscible liquids, in spite of the nonlinearity of the chain connectivity.

We observed an attractive fluctuation-induced force between the rings for all the studied cases. We characterize these forces as a function of chain stretching, temperature, and ring radius, i.e., the properties of the physical constraint imposed on the chain. For higher stretching, we found a dependence of $\sim 1/d$ of the fluctuation-induced force, which is similar to that found in the context of a harmonic approximation for classical electromagnetic fields at thermal equilibrium [41], and the 2D Ising model of a pinned magnetic interface [45]. We observed a linear dependence of the force with the temperature, which is expected from an entropy-driven force of this type, if the entropy differences between the constraint and the unconstrained chains are not dependent on temperature.

At lower stretchings, in which not all the degrees of freedom of the chain are vibrating, we observe a deviation from this limiting behavior. In this case, the force versus distance is adjusted very well with a dependence $\sim 1/d \ln(c_1 d)$. This behavior was also found theoretically in the exact results for interfaces of 3D Ising systems [45] and for colloids pinned in liquid-liquid interfaces [9]. We also characterized fluctuations of the force at very high stretchings, coming from the discreteness of the beads and variations of the excluded volume of the chain along the bonds.

In addition to the results found for polymers under tension, we consider the system as a relatively simple model to study fluctuation-induced forces in different contexts. We are planning to continue this work by studying the dynamics of rings that are allowed to move in the direction of the chain, and also by considering semiflexible polymers with local flexural rigidity, reminiscent of biofilaments. For this case, there is an increment in the length of bond correlations, which could be very interesting. We are also planning to study the aggregation of ring molecules threaded in the chain, in a system closer to a polyrotaxane. Finally, we think that the direct measurement of these forces with optical tweezers is plausible, or via a potential of mean force in fluorescence experiments [46,47].

ACKNOWLEDGMENTS

C.P. warmly thanks M. Müller for enjoyable and fruitful discussions during the development of this work. A. de Virgillis, with whom we exchanged many ideas on the system studied here, is also gratefully acknowledged. C.P. also gratefully acknowledges encouraging discussions with K. Binder and T. Kreer in the early stages of this work. This research was supported by CONICET (PIP 112 201101004 64), MINCYT (PICT-E 2014, PICT 1887-2011), and CNEA (INN-CNEA 2011). R.L thanks UTN for the support via a Ph.D scholarship (UTN Rectorado Res. 1351/14).

F.M.G. and R.L. contributed to this work on an equal basis.

[1] H. B. G. Casimir, Proc. K. Ned. Akad. Wet. **51**, 793 (1948).
[2] M. Kardar and R. Golestanian, Rev. Mod. Phys. **71**, 1233 (1999).
[3] *Casimir Physics*, 1st ed., edited by D. Dalvit, P. Milonni, D. Roberts, and F. da Rosa, Lecture Notes in Physics Vol. 834 (Springer-Verlag, Berlin, 2011).
[4] A. O. Sushkov, W. J. Kim, D. A. R. Dalvit, and S. K. Lamoreaux, Nat. Phys. **7**, 230 (2011).
[5] M. E. Fisher and P. G. de Gennes, C. R. Acad. Sci., Ser. B **287**, 207 (1978).
[6] C. Hertlein, L. Helden, A. Gambassi, S. Dietrich, and C. Bechinger, Nature (London) **451**, 172 (2008).
[7] A. Gambassi, J. Phys.: Conf. Ser. **161**, 012037 (2009).
[8] S. K. Lamoreaux, Phys. Today **60**(2), 40 (2007).
[9] H. Lehle, M. Oettel, and S. Dietrich, Europhys. Lett. **75**, 174 (2006).
[10] F. Bresme, H. Lehle, and M. Oettel, J. Chem. Phys. **130**, 214711 (2009).
[11] T. R. Weikl, Europhys. Lett. **54**, 547 (2001).

[12] B. B. Machta, S. L. Veatch, and J. P. Sethna, Phys. Rev. Lett. **109**, 138101 (2012).
[13] A. Ganshin, S. Scheidemantel, R. Garcia, and M. H. W. Chan, Phys. Rev. Lett. **97**, 075301 (2006).
[14] R. Garcia and M. H. W. Chan, Phys. Rev. Lett. **83**, 1187 (1999).
[15] B. J. Reynwar and M. Deserno, Biointerphases **3**, FA117 (2008).
[16] H.-K. Lin, R. Zandi, U. Mohideen, and L. P. Pryadko, Phys. Rev. Lett. **107**, 228104 (2011).
[17] E. Noruzifar and M. Oettel, Phys. Rev. E **79**, 051401 (2009).
[18] E. Noruzifar, J. Wagner, and R. Zandi, Phys. Rev. E **88**, 042314 (2013).
[19] A. Aminov, Y. Kafri, and M. Kardar, Phys. Rev. Lett. **114**, 230602 (2015).
[20] D. Ray, C. Reichhardt, and C. J. Olson Reichhardt, Phys. Rev. E **90**, 013019 (2014).
[21] C. Parra-Rojas and R. Soto, Phys. Rev. E **90**, 013024 (2014).
[22] J. Araki and K. Ito, Soft Matter **3**, 1456 (2007).
[23] E. M. Sevick and D. R. M. Williams, Langmuir **26**, 5864 (2010).
[24] Y. Noda, Y. Hayashi, and K. Ito, J. Appl. Polym. Sci. (to be published).
[25] K. Ito, Curr. Opin. Solid State Mater. Sci. **14**, 28 (2010).
[26] K. Kato, T. Yasuda, and K. Ito, Polymer **55**, 2614 (2014).
[27] G. S. Grest and K. Kremer, Phys. Rev. A **33**, 3628 (1986).
[28] K. Kremer and G. S. Grest, J. Chem. Phys. **92**, 5057 (1990).
[29] C. Pastorino, K. Binder, T. Kreer, and M. Müller, J. Chem. Phys. **124**, 064902 (2006).
[30] C. Pastorino, K. Binder, and M. Müller, Macromolecules **42**, 401 (2009).
[31] G. Grest, Adv. Polym. Sci. **138**, 1 (1999).
[32] J. Baschnagel and F. Varnik, J. Phys.: Condens. Matter **17**, R851 (2005).
[33] M. Kroger, Phys. Rep.-Rev. Sec. Phys. Lett. **390**, 453 (2004).
[34] M. Febbo, A. Milchev, V. Rostiashvili, D. Dimitrov, and T. A. Vilgis, J. Chem. Phys. **129**, 154908 (2008).
[35] P. Hünenberger, Adv. Polym. Sci. **173**, 105 (2005).
[36] C. Pastorino, T. Kreer, M. Müller, and K. Binder, Phys. Rev. E **76**, 026706 (2007).
[37] H. J. Pain, *The Physics of Vibrations and Waves* (Wiley, Chichester, 2005).
[38] R. L. C. Vink, J. Horbach, and K. Binder, J. Chem. Phys. **122**, 134905 (2005).
[39] S. Safran, *Statistical Thermodynamics of Surfaces, Interfaces, and Membranes* (Westview, Boulder, CO, 2003).
[40] J. Israelachvili, *Intermolecular and Surface Forces* (Academic Press, Burlington, MA, 2011).
[41] T. H. Boyer, J. Phys. A **36**, 7425 (2003).
[42] T. H. Boyer, Am. J. Phys. **71**, 990 (2003).
[43] N. Ashcroft, *Solid State Physics* (Holt, Rinehart and Winston, New York, 1976).
[44] R. Golestanian, M. Goulian, and M. Kardar, Phys. Rev. E **54**, 6725 (1996).
[45] D. B. Abraham, F. H. L. Essler, and A. Maciołek, Phys. Rev. Lett. **98**, 170602 (2007).
[46] C. Bustamante, Annu. Rev. Biochem. **77**, 45 (2008).
[47] D. H. Goldman, C. M. Kaiser, A. Milin, M. Righini, I. Tinoco, and C. Bustamante, Science **348**, 457 (2015).